Nonlinear Dynamics

Laurette TUCKERMAN

laurette@pmmh.espci.fr

Maps, Period Doubling and Floquet Theory

1 Discrete Dynamical Systems or Mappings

A discrete dynamical system is of the form

$$y_{n+1} = g(y_n) \tag{1}$$

where y and g are real vectors of the same dimension. A fixed point of (1) is a solution to

$$\bar{y} = g(\bar{y}) \tag{2}$$

In one dimension, linear stability analysis of $\bar{y}$ is carried out by writing

$$
\begin{aligned}
y_n &= \bar{y} + \epsilon_n \\
y_{n+1} &= g(y_n) \\
\bar{y} + \epsilon_{n+1} &= g(\bar{y} + \epsilon_n) \\
&= g(\bar{y}) + g'(\bar{y})\epsilon_n + \frac{1}{2}g''(\bar{y})\epsilon_n^2 \cdots \\
\epsilon_{n+1} &\approx g'(\bar{y})\epsilon_n
\end{aligned}
\tag{3}
$$

We see that $|\epsilon|$ decreases, i.e. $\bar{y}$ is a stable fixed point, if $|g'(\bar{y})| < 1$ and that $|\epsilon|$ grows, i.e. $\bar{y}$ is an unstable fixed point, if $|g'(\bar{y})| > 1$.

If $g'\bar{y}) = 0$, then $\bar{y}$ is said to be *superstable*, with very fast convergence to the fixed point:

$$\epsilon_{n+1} \approx \frac{1}{2}g''(\bar{y})\epsilon_n^2 \tag{4}$$

In a multidimensional system, $g'(\bar{y})$ is replaced by the Jacobian $Dg(\bar{y})$ and $\bar{y}$ is a stable fixed point if all of the eigenvalues μ of $Dg(\bar{y})$ satisfy $|\mu| < 1$, i.e. are inside the unit circle.

Loss of stability can take place in three different ways, as illustrated in figure 1:

i) An eigenvalue may exit the unit circle at $(1, 0)$.

ii) A complex conjugate pair of eigenvalues may exit the unit circle at $e^{\pm i\theta}$.

iii) An eigenvalue may exit the unit circle at $(-1, 0)$.

We illustrate cases (i) and (iii) using a graphical construction for iterating maps. We draw graphs of $f(x)$ and the diagonal line ($y = x$). We draw a vertical line from the x-axis at x_0 up to $f(x_0)$, then a horizontal line across to $y = x$, then a vertical line down to the x-axis at x_1 and then repeat this procedure to iterate the map. (We can combine the two consecutive vertical lines, i.e. drawing the vertical line directly to the $f(x)$ curve instead of to the x-axis.)

$$(x_0, 0) \to (x_0, x_1 \equiv f(x_0)) \to (x_1, x_1) \to (x_1, x_2 \equiv f(x_1)) \to \cdots \tag{5}$$

Figure 2 shows trajectories resulting from iterating linear maps $f(x) = cx$ for values of c which are positive and negative, and with absolute value greater and less than one. There is a fixed point at $\bar{x} = 0$. This fixed point is stable if $|c| < 1$, unstable if $|c| > 1$. Trajectories proceed monotonically if $c > 0$ and oscillate between values to the right and left of $\bar{x}$ if $c < 0$.
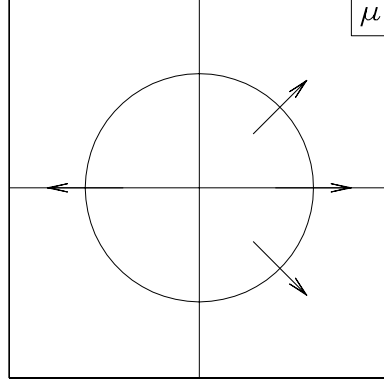
Figure 1: Eigenvalues (or complex conjugate pairs of eigenvalues) can exit the unit circle in three ways: at (1,0), at $e^{\pm i\theta}$ or at (-1,0).

Loss of stability is associated with various types of bifurcations. Case (i), when eigenvalues cross at $+1$, leads to a steady bifurcation, analogous to those seen for continuous dynamical systems. The steady bifurcation may be a saddle-node, a pitchfork, or a transcritical bifurcation. We can write simple equations that display steady bifurcations analogous to those found for flows.

Saddle-node bifurcation:

$$\dot{x} \rightarrow x_{n+1} - x_n = \mu - x_n^2 \qquad \Longrightarrow \qquad x_{n+1} = f(x_n) = x_n + \mu - x_n^2 \tag{6}$$

Fixed points $\pm\sqrt{\mu}$ satisfying $f(\bar{x}) = \bar{x}$ exist for $\mu > 0$. Their stability is calculated via

$$
\begin{aligned}
f(x) &= x + \mu - x^2 \\
f'(x) &= 1 - 2x \\
f'(\pm\sqrt{\mu}) &= 1 \mp 2\sqrt{\mu} \lessgtr 1 \text{ for } \mu > 0
\end{aligned}
\tag{7}
$$

Pitchfork bifurcation:

$$\dot{x} \rightarrow x_{n+1} - x_n = \mu x_n - x_n^3 \qquad \Longrightarrow \qquad x_{n+1} = f(x_n) = x_n + \mu x_n - x_n^3 \tag{8}$$

The fixed points $0, \pm\sqrt{\mu}$ satisfy $f(\bar{x}) = \bar{x}$. Their stability is calculated via

$$
\begin{aligned}
f(x) &= x + \mu x - x^3 \\
f'(x) &= 1 + \mu - 2x^2 \\
f'(0) &= 1 + \mu \lessgtr 1 \text{ for } \mu \lessgtr 0 \tag{9}\\
f'(\pm\sqrt{\mu}) &= 1 - \mu < 1 \text{ for } \mu > 0 \tag{10}
\end{aligned}
$$

Subcritical pitchfork bifurcations and transcritical bifurcations can also occur. Saddle-node and pitchfork (super and subcritical) bifurcations are illustrated in figure 3.

Case (ii), when eigenvalues cross at $e^{\pm i\theta}$, leads to a secondary Hopf, or Neimark-Sacker, bifurcation to a torus. We will discuss this in the next chapter. Case (iii), when eigenvalues cross at -1 leads to a flip, or a period-doubling bifurcation, and is a phenomenon that cannot occur for continuous dynamical systems. We now discuss this case in the context of the logistic map.
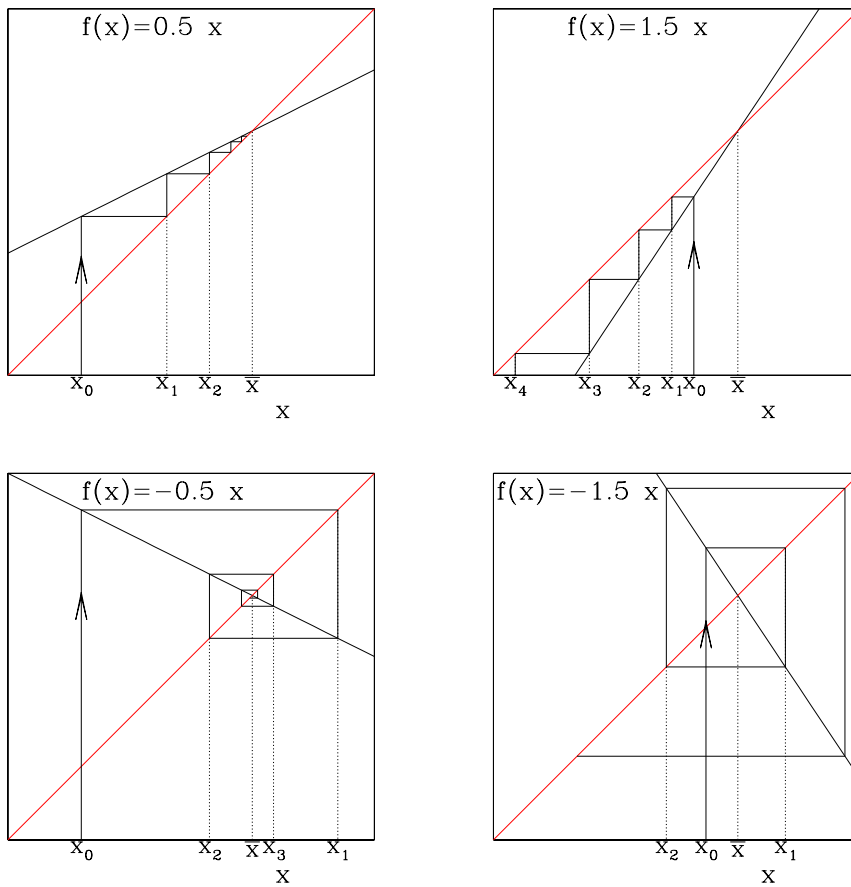
Figure 2: Graphical construction for iterating maps. $f(x) = cx$ with various slopes c.
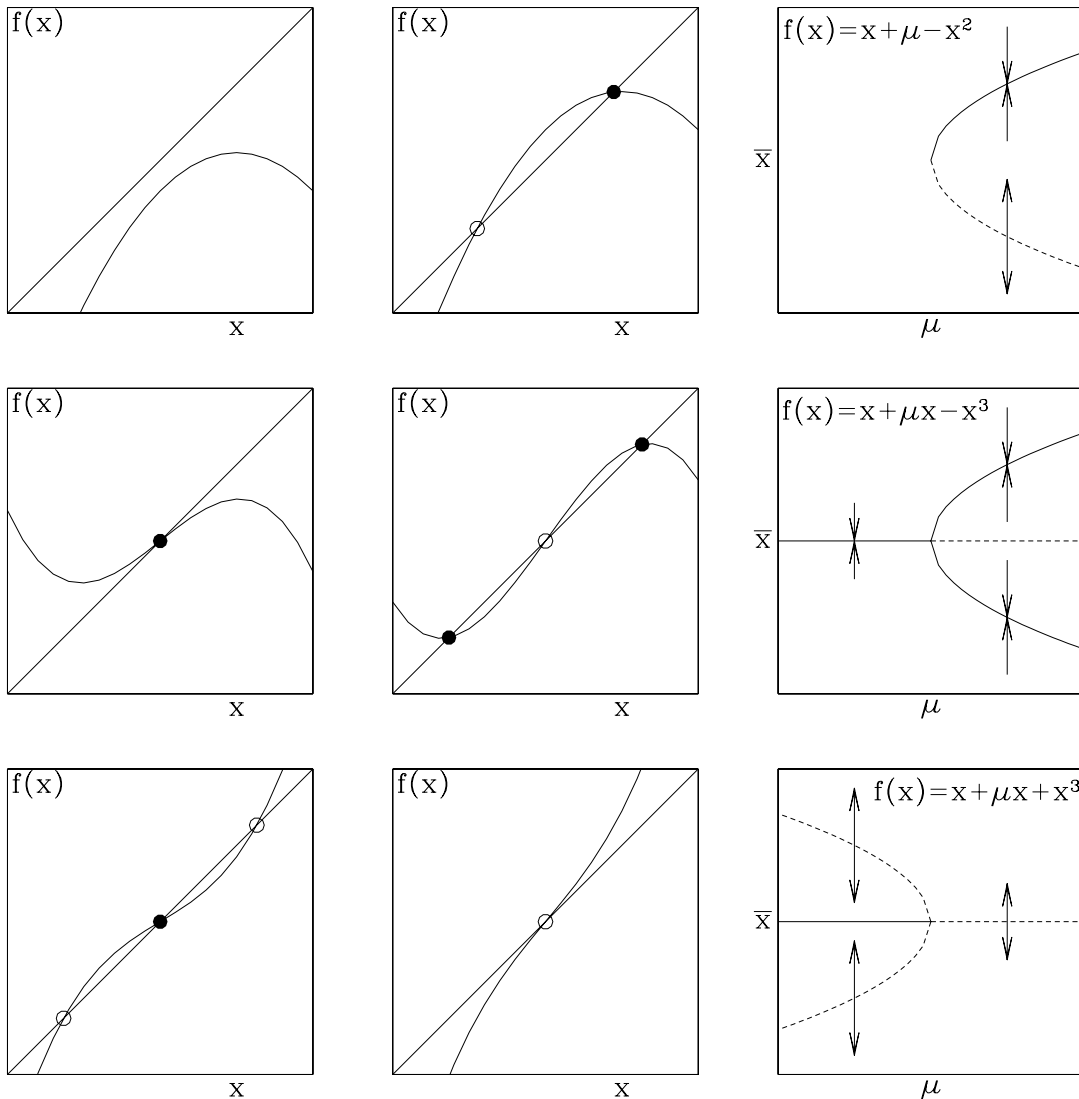
Figure 3: Steady bifurcations for discrete dynamical systems.
Top row: Saddle-node bifurcation. $f(x) = x + \mu - x^2$ for $\mu = -0.2$ (left) and for $\mu = 0.2$ (middle).
Middle row: Supercritical pitchfork. $f(x) = x + \mu x - x^3$ for $\mu = -0.2$ (left) and for $\mu = 0.4$ (middle).
Bottom row: Subcritical pitchfork. $f(x) = x + \mu x + x^3$ for $\mu = -0.4$ (left) and for $\mu = 0.2$ (middle).
Right: corresponding bifurcation diagrams.

2 Logistic Map

The logistic map was proposed in the 1800s and popularized in the 1970s as a model for population biology. Population growth is geometric (the next value is a multiple of the current value) when the population is small, but is reduced when the population is too large. It is with this map that the famous period-doubling cascade was discovered, also in the 1970s, by Feigenbaum in Los Alamos, U.S. and, almost simultaneously, by Coullet and Tresser in Nice, France.
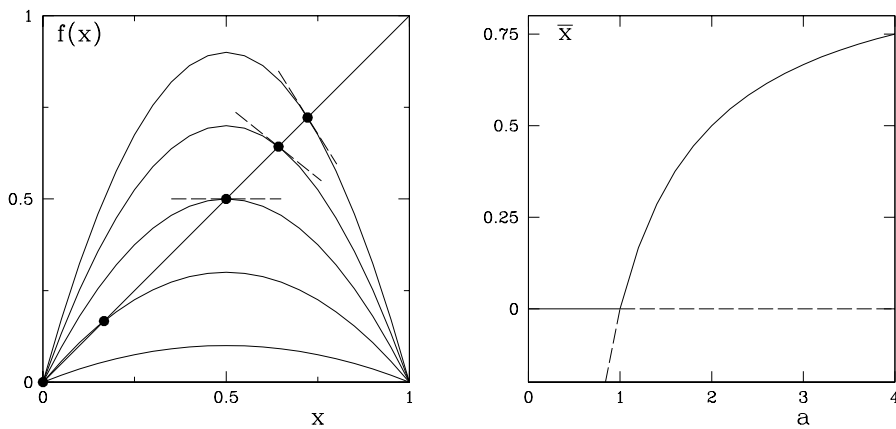
2.1 Fixed points and period doubling

Figure 4: Left: the logistic map $f(x) = ax(1 - x)$ for $a = 0.4$, 1.2, 2.0, 2.8, 3.6. Fixed points (dots) are located at $\bar{x} = 0$ and $\bar{x} = 1 - 1/a$. Short dashed line segments have slope $f'(\bar{x})$.
Right: fixed points $\bar{x} = 0$ and $\bar{x} = 1 - 1/a$ as a function of a.

The logistic map is defined by:

$$x_{n+1} = f(x_n) \equiv ax_n(1 - x_n) \qquad \text{for } x_n \in [0, 1], \qquad 0 < a < 4 \tag{11}$$

f is a quadratic function mapping $[0, 1]$ into itself, with minima at the two endpoints $f(0) = f(1) = 0$ and a maximum at the midpoint $f(1/2) = a/4$. Its fixed points are easily calculated:

$$\bar{x} = a\bar{x}(1 - \bar{x}) \qquad \Longrightarrow \begin{cases} \bar{x} = 0 & \text{or} \\ 1 = a(1 - \bar{x}) \Longrightarrow 1 - \bar{x} = 1/a \Longrightarrow \bar{x} = 1 - 1/a \end{cases} \tag{12}$$

These are shown in figure 4.

The stability of these fixed points is also easily determined:

$$
\begin{aligned}
f(x) &= ax(1-x) \\
f'(x) &= a(1-x) - ax = a(1-2x) \\
f'(0) &= a \implies |f'(0)| < 1 \text{ for } a < 1 \\
f'\left(1 - \frac{1}{a}\right) &= a\left(1 - 2\left(1 - \frac{1}{a}\right)\right) = a\left(-1 + \frac{2}{a}\right) = -a + 2 \\
-1 &< f'\left(1 - \frac{1}{a}\right) < 1 \\
-1 &< -a + 2 < 1 \\
-1 &< a - 2 < 1 \\
1 &< a < 3
\end{aligned}
\tag{13}
$$

Thus, events must occur at $a = 1$ and at $a = 3$ in order for $\bar{x} = 1 - 1/a$ to change stability. The event which occurs at $a = 1$ can be seen to be a transcritical bifurcation from the right portion of figure 4 and from (13): when the two fixed points intersect at $a = 1$, they exchange stabilities. (However, $\bar{x} = 1 - 1/a$ is outside of the domain $[0, 1]$ for $a < 1$.)

In figure 5 we illustrate the fixed points and their stability using the graphical construction.

We now turn our attention to understanding what happens at $a = 3$, at which $f'(\bar{x}) = -1$, which causes $\bar{x} = 1 - 1/(a)$ to become unstable. Guided by figure 5, we seek a two-cycle, i.e. values $x_{1,2}$ for which $f(x_1) = x_2$ and $f(x_2) = x_1$, so that $f(f(x_1)) = x_1$ and $f(f(x_2)) = x_2$. We denote the composition of f with itself, i.e. $f(f(x))$, by $f^2(x)$. We compute:

$$
\begin{aligned}
f^2(x) &= af(x)(1 - f(x)) \\
&= a\left(ax(1-x)\right)\left[1 - ax(1-x)\right] \\
&= a^2 x(1-x)\left[1 - ax + ax^2\right] \\
&= a^2 x\left[1 - ax + ax^2 - x + ax^2 - ax^3\right] \\
&= a^2 x\left[1 - (1+a)x + 2ax^2 - ax^3\right]
\end{aligned}
\tag{14}
$$

We seek fixed points of f^2, i.e. roots of

$$
f^2(x) - x = x\left[a^2(1 - (1+a)x + 2ax^2 - ax^3) - 1\right]
\tag{15}
$$

Solving (15) is facilitated by the fact that we already know two roots, namely $x = 0$ and $x = 1 - 1/a$, since $f(\bar{x}) = \bar{x}$ implies $f^2(\bar{x}) = \bar{x}$. Therefore, the quartic polynomial in (15) contains as factors x and $x - (1 - 1/a)$ or $(a(x-1) + 1)$. In fact:

$$
f^2(x) - x = -ax(a(x-1) + 1)\left[ax^2 - (a+1)x + (a+1)/a\right]
\tag{16}
$$

The additional roots of (16) are

$$
x_{1,2} = \frac{a + 1 \pm \sqrt{(a-3)(a+1)}}{2a}
\tag{17}
$$

For $a < 3$, the argument of the square root is negative and so f^2 has no additional real roots and hence no two-cycle. At $a = 3$, we have $a - 3 = 0$ and so $x_{1,2} = (a+1)/(2a) = 2/3$. A graph of $f^2(x)$ and the new fixed points $x_{1,2}$. is shown in figure 6. We see that f^2 undergoes a pitchfork bifurcation.
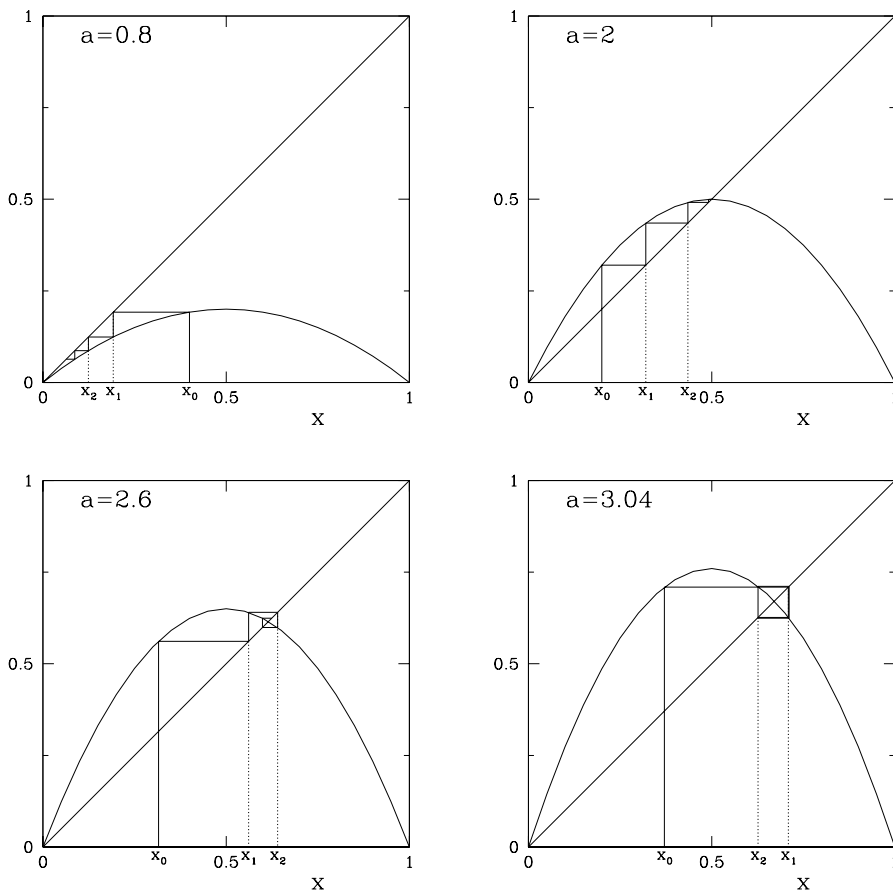
Figure 5: Behavior of the logistic map. For $a = 0.8$, $x_n \to 0$. For $a = 2.0$ and $a = 2.6$, $x_n \to \bar{x} = 1 - 1/a$. For $a = 3.04$, x_n converges to a two-cycle.
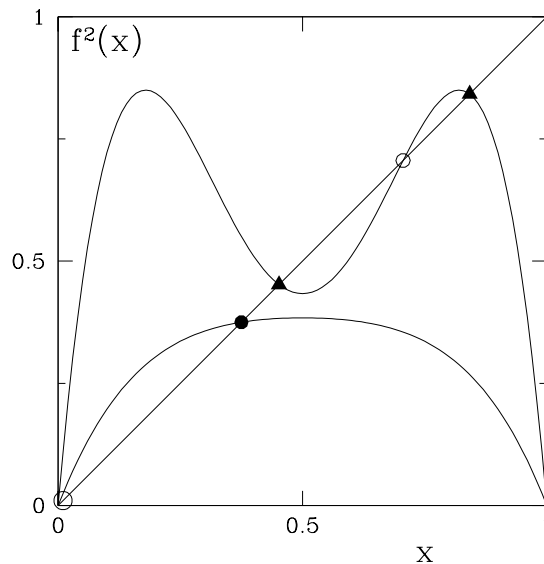

Figure 6: Graph of $f^2(x)$, where $f(x) = 1 - ax(1 - x)$, and of $y = x$. For $a = 1.6$, f^2 has the same fixed points as f, namely $x = 0$ (unstable, hollow dot) and $x = 1 - 1/(a)$ (stable, filled dot). For $a = 3.4$, the fixed point $x = 1 - 1/a$ has become unstable and two new fixed points $x_{1,2}$ (filled triangles) have appeared, which together comprise a two-cycle for f.

We will need:

$$x_1 + x_2 = 1 + \frac{1}{a} = \frac{a+1}{a} \tag{18}$$

$$x_1 x_2 = \frac{a+1}{a^2} \tag{19}$$

As you might be beginning to guess, we can continue this process and check for stability of the two-cycle. We have:

$$\frac{d}{dx} f^2(x) = f'(f(x)) f'(x) \tag{20}$$

For an element of a two-cycle

$$\frac{d}{dx} f^2(x_1) = f'(x_2) f'(x_1) \tag{21}$$

For the two-cycle (17), we have

$$
\begin{aligned}
f'(x_1) f'(x_2) &= a(1 - 2x_1)\, a(1 - 2x_2) \\
&= a^2 (1 - 2(x_1 + x_2) + 4 x_1 x_2) \\
&= a^2 \left(1 - 2\left(\frac{a+1}{a} \right) + 4\left(\frac{a+1}{a^2} \right) \right) \\
&= a^2 - 2a(a+1) + 4(a+1) \\
&= -a^2 + 2a + 4
\end{aligned}
\tag{22}
$$

$$
\begin{aligned}
0 &= f'(x_1) f'(x_2) - 1 = -a^2 + 2a + 4 - 1 = -a^2 + 2a + 3 \\
a &= \frac{2 \pm \sqrt{4 + 12}}{2} = \frac{2 \pm \sqrt{16}}{2} = \frac{2 \pm 4}{2} = 3
\end{aligned}
\tag{23}
$$

$$
\begin{aligned}
0 &= f'(x_1) f'(x_2) + 1 = -a^2 + 2a + 4 + 1 = -a^2 + 2a + 5 \\
a &= \frac{2 \pm \sqrt{4 + 20}}{2} = \frac{2 + \sqrt{24}}{2} = \frac{2 + 2\sqrt{6}}{2} = 1 + \sqrt{6} = 3.44948\ldots
\end{aligned}
\tag{24}
$$

where we have discarded the negative value of r in (24). Equation (23) confirms that the two-cycle of f, a fixed point of f^2, is created via a steady-state (pitchfork) bifurcation at $a = 3$. Equation (24) states that this two-cycle loses stability via a flip bifurcation at $a = 3.44948\ldots$, leading to a four-cycle.

The successive period-doubling bifurcations occur at successively smaller intervals in r and *accumulate* at $a = 3.569945672\ldots$, as shown in table 1. This is called the *period-doubling cascade*.

2.2 Renormalization

The behavior of the logistic map is actually *universal*. The qualitative and quantitative properties above (specifically, the value of δ in Table 1) hold for any family of maps with a quadratic maximum, such as $r \sin \pi x$ Why should this be? Feigenbaum and Coullet and Tresser provided an explanation of the period-doubling cascade in terms of *renormalization*. The idea is that the interior portion of f^2 resembles a scaled version of f. To facilitate the calculations, we use the map

$$f(x) = 1 - ax^2 \tag{25}$$

9

n	2^n	a_n	$\Delta_n \equiv a_n - a_{n-1}$	$\delta_n \equiv \Delta_{n-1}/\Delta_n$
0	1	1		
1	2	3	2	
2	4	3.44948	0.449	4.45
3	8	3.54408	0.0948	4.747
4	16	3.56872	0.0244	4.640
5	32	3.5698912	0.00116	4.662
$\vdots$	$\vdots$	$\vdots$	$\vdots$	$\vdots$
∞	∞	3.569945672	0	4.669

Table 1: Period-doubling cascade for logistic map.

on the interval $[-1, 1]$, shown in figure 7. Figure 7 also shows $f^2(x)$ and a box surrounding the central minimum of f^2. The idea is that the portion of f^2 inside the box, when scaled horizontally and vertically, resembles f. Specifically, figure 7 also shows

$$Tf(x) \equiv -\frac{1}{\alpha}f^2(-\alpha x) \tag{26}$$

The resemblance is quantified as follows:

$$
\begin{aligned}
f(x) &\approx Tf(x) \tag{27}\\
1 - ax^2 &\approx -\frac{1}{\alpha}f^2(-\alpha x)\\
&= -\frac{1}{\alpha}f(1 - a(\alpha x)^2)\\
&= -\frac{1}{\alpha}(1 - a(1 - a(\alpha x)^2)^2)\\
&= -\frac{1}{\alpha}(1 - a(1 - 2a(\alpha x)^2 + a^2(\alpha x)^4))\\
&= -\frac{1}{\alpha}(1 - a + 2a^2(\alpha x)^2 - a^3(\alpha x)^4) \tag{28}
\end{aligned}
$$

For the constant and quadratic terms in (28) to agree, we require

$$
\begin{aligned}
\frac{a-1}{\alpha} &= 1 & \frac{2a^2\alpha^2}{\alpha} &= a\\
a - 1 &= \alpha & 2a\alpha &= 1\\
& & 2a(a-1) &= 1\\
\alpha &= 0.366 & a &= \frac{1 + \sqrt{3}}{2} = 1.366 \tag{29}
\end{aligned}
$$

The dashed curve in figure 7 is $Tf(x)$ with the parameters of (29). To go from f^2 to f^4, or more generally from f^{2^n} to $f^{2^{n+1}}$, we would repeat this procedure. At each stage the scaling factor α_n is set to $\alpha_n = -f^{2^n}(\pm 1)$ and a_n is determined by an equation like (27). Tf is not a quadratic polynomial like f (25), but a quartic polynomial; T^2f is an eighth-order polynomial, and so on. It has been shown that this procedure converges to a function

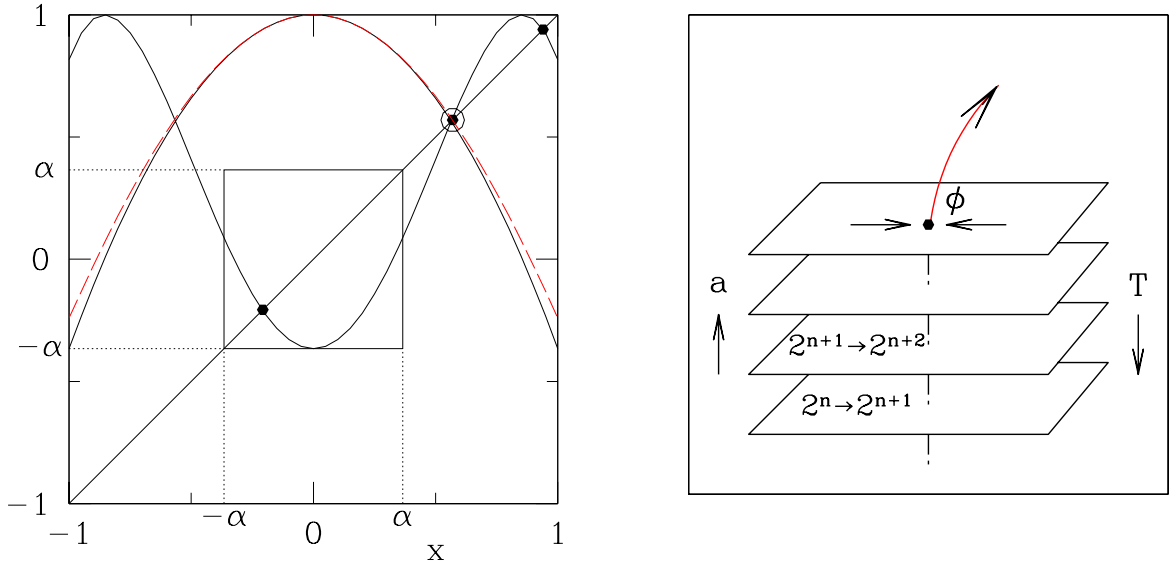$$\phi(x) = 1 - 1.528\ldots x^2 + 0.105\ldots x^4 + 0.0267\ldots x^6 + \ldots \tag{30}$$

10

Figure 7: Left: Graph of $f(x) = 1 - ax^2$, of $f^2(x)$, and of $Tf(x) \equiv -\frac{1}{\alpha}f^2(-\alpha x)$ (dashed curve). $Tf(x)$ consists of the portion of f^2 inside the box, rescaled by α. Fixed points of f^2 and Tf are indicated by solid dots and hollow dots, respectively. Parameters are $a = 1.366$ and $\alpha = 0.366$. Right: Schematic diagram of action of T on space of mappings. Each sheet consists of mappings that are just undergoing a period-doubling bifurcation from 2^n to 2^{n+1}. The fixed point ϕ is a mapping with one unstable direction under the action of T.

We view T as itself a mapping on mappings, with ϕ a fixed point of T. The fixed point has a single unstable direction, with multiplier $\delta = 4.6692\ldots$, the same value found in the last column of table 1. The scaling coefficients α_n also converge to the universal value of $2.50280787\ldots$.

2.3 Periodic Windows

Periodic windows are created when f^n traverses the diagonal, undergoing one or more saddle-node bifurcations and creating fixed points of f^n, which are n-cycles of f. Necessarily, the new fixed points are created in pairs, and necessarily, one is stable and one is unstable. Figure 8 shows this for a three-cycle.

The n-cycles each undergo period-doubling and, in fact, an entire period-doubling sequence. Below the saddle-node bifurcation which creates them, one can see *intermittency*, where the trajectories spend a long time in the vicinity of the "ghosts" of the n-cycles, i.e. slow regions in which the n-cycles will appear but have not yet done so. Figure 10 shows this for a three-cycle. The three-cycle exists and is stable for $1 + \sqrt{8} = 3.828427 < r < 3.857$.
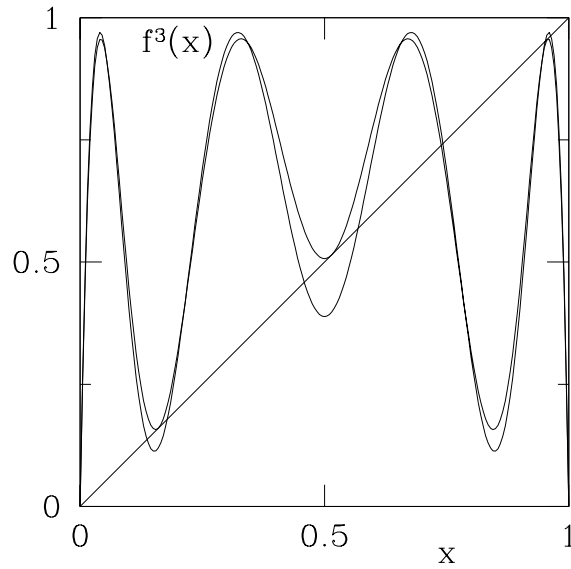
11

Figure 8: f^3 for $a = 3.8496$ and $a = 3.88$. f^3 undergoes three saddle-node bifurcations at $a_3 = 3.8496$. For a above this value, f has two 3-cycles, one stable ($|(f^3)'| < 1$) and one unstable ($|(f^3)'| > 1$).
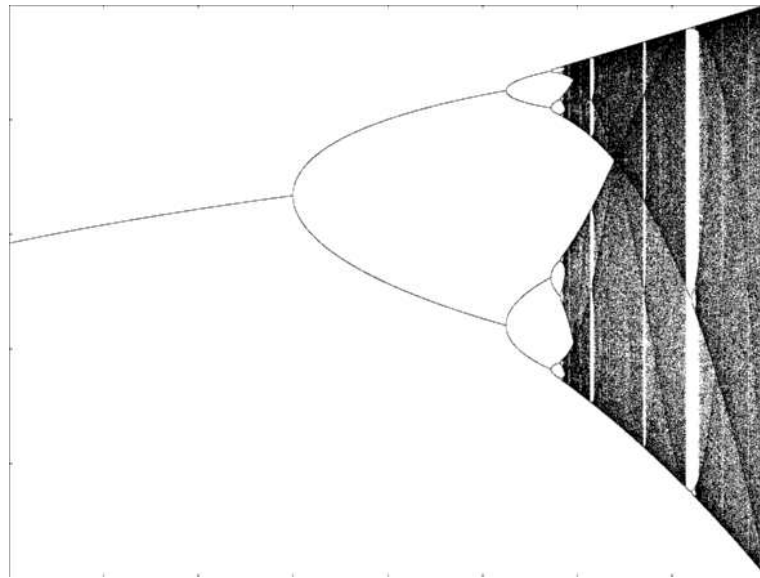

Figure 9: Bifurcation diagram for logistic map, showing period-doubling cascade and periodic windows. Shown are fixed points or elements of cycles as a function of r.
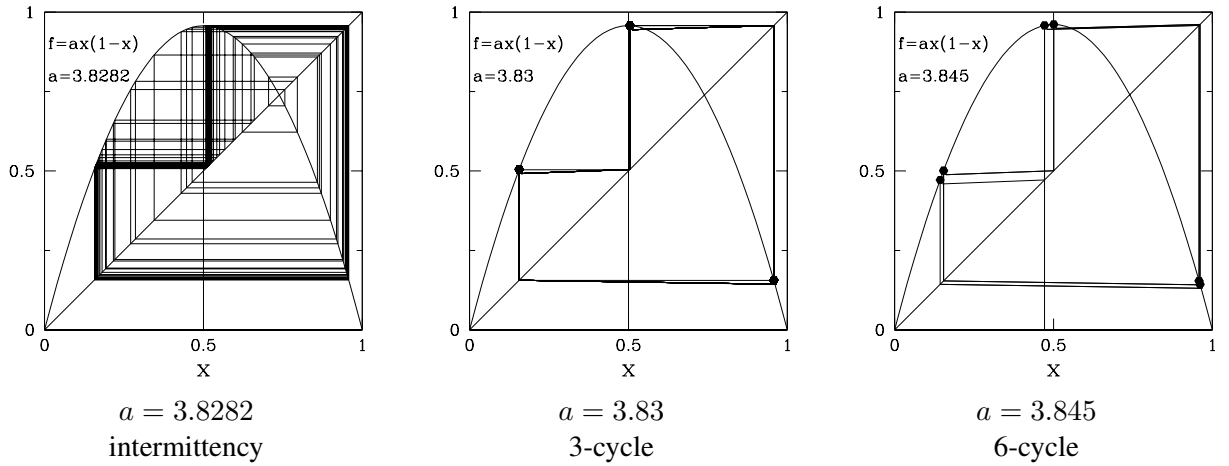
| $a = 3.8282$ | $a = 3.83$ | $a = 3.845$ |
| intermittency | 3-cycle | 6-cycle |

Figure 10: Below, during, and after a three-cycle

We order the positive integers as follows:

$$3 \triangleright 5 \triangleright 7 \triangleright 9 \ldots$$
$$2 \cdot 3 \triangleright 2 \cdot 5 \triangleright 2 \cdot 7 \triangleright 2 \cdot 9 \ldots$$
$$2^2 \cdot 3 \triangleright 2^2 \cdot 5 \triangleright 2^2 \cdot 7 \triangleright 2^2 \cdot 9 \ldots$$
$$\ldots 2^3 \triangleright 2^2 \triangleright 2 \triangleright 1 \tag{31}$$

This is called the Sharkovskii order. Sharkovskii's Theorem states that if f has a k-cycle, then it an ℓ-cycles for any $\ell \triangleright k$. In particular, if f has a 3-cycle, then it has cycles of all lengths. This theorem says nothing, in either the hypothesis or the conclusion, about the stability of any of these cycles.

The logistic map has a 3-cycle, which originates in three simultaneous saddle-node bifurcations at $r_3 = (1 + \sqrt{8})/4 = 0.9624$. This is illustrated in figure 8. Therefore, by Sharkovskii's Theorem, the logistic map for any $r > r_3$ has cycles of *all* lengths.

2.4 Tent Map and Shift Map

Other classes of *unimodal maps*, characterized by the nature of their extrema, undergo a period-doubling cascade. Each class has its own asymptotic value of δ and α. Examples are functions with a quartic maximum and the *tent map*

$$f(x) = \begin{cases} 2rx & \text{for } x < 1/2 \\ 2r(1 - x) & \text{for } x > 1/2 \end{cases} \tag{32}$$

shown in figure 11.

Consider the logistic mapping with $a = 4$

$$x_{n+1} = 4x_n(1 - x_n) \tag{33}$$

transformed to a new variable $0 \leq y_n \leq 1$ via
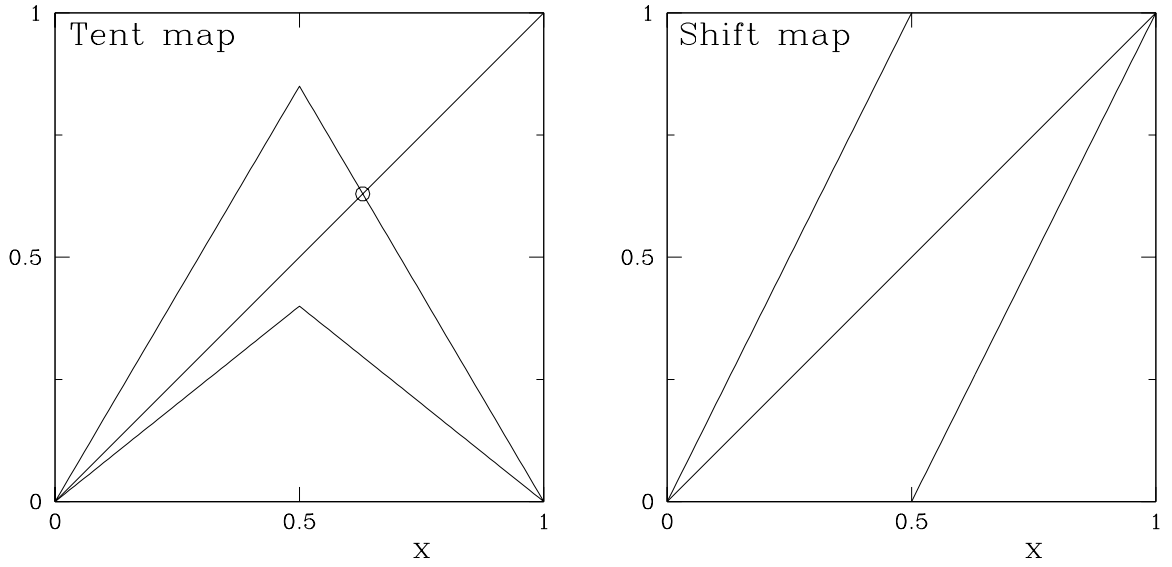
$$x_n = \sin^2(2\pi y_n) \tag{34}$$

13

Figure 11: Left: Tent map (32) for $r = 0.4$ and $r = 0.85$. The origin is a fixed point, stable for $r < 0.5$ and unstable for $r > 0.5$. For $r > 0.5$, there is another fixed point, $\bar{x} = 2r/(1 + 2r)$. Right: Shift map (36).

We have

$$
\begin{aligned}
\sin^2(2\pi y_{n+1}) &= 4\sin^2(2\pi y_n)(1 - \sin^2(2\pi y_n)) \\
&= 4\sin^2(2\pi y_n)\cos^2(2\pi y_n) \\
&= (2\sin(2\pi y_n)\cos(2\pi y_n))^2 \\
&= (\sin(4\pi y_n))^2 \\
\sin(2\pi y_{n+1}) &= \sin(4\pi y_n) \\
2\pi y_{n+1} &= 4\pi y_n + 2k\pi \\
y_{n+1} &= 2y_n + k
\end{aligned}
\tag{35}
$$

This is called the *shift mapping*

$$
y_{n+1} = 2y_n \bmod 1 \tag{36}
$$

because if we write y_n in binary notation, the action of the mapping is to *shift* the digits of y, losing the leading digit each time. From this we can easily make k-cycles, just by writing repeating patterns of k binary digits. Since the set of non-repeating numbers is of measure one, so is the set of initial conditions leading to chaotic trajectories.

14

3 Fluid-dynamical examples

3.1 Rayleigh-Bénard convection: period-doubling cascade

The first observation of a period-doubling cascade in a fluid-dynamical experiment was made by Libchaber, Fauve and Laroche at ENS in Paris in the early 1980s. An electrically conducting fluid (mercury), was subjected to both a vertical temperature gradient (Rayleigh-Bénard convection) and a horizontal magnetic field. Timeseries and temporal power spectra from the experiment are shown in figure 12. The timeseries show periods 2, 4, 8, 16. To understand the power spectra, it is important to recall that harmonics are always present: a periodic signal is generally not sinusoidal. Such harmonics are generally of much lower magnitude. Power spectrum A shows the main frequency f and its subharmonic $f/2$. Multiples of these are present with lower amplitudes. Power spectrum B shows f, $f/2$ and $f/4$. Multiples of these are present with lower amplitudes.
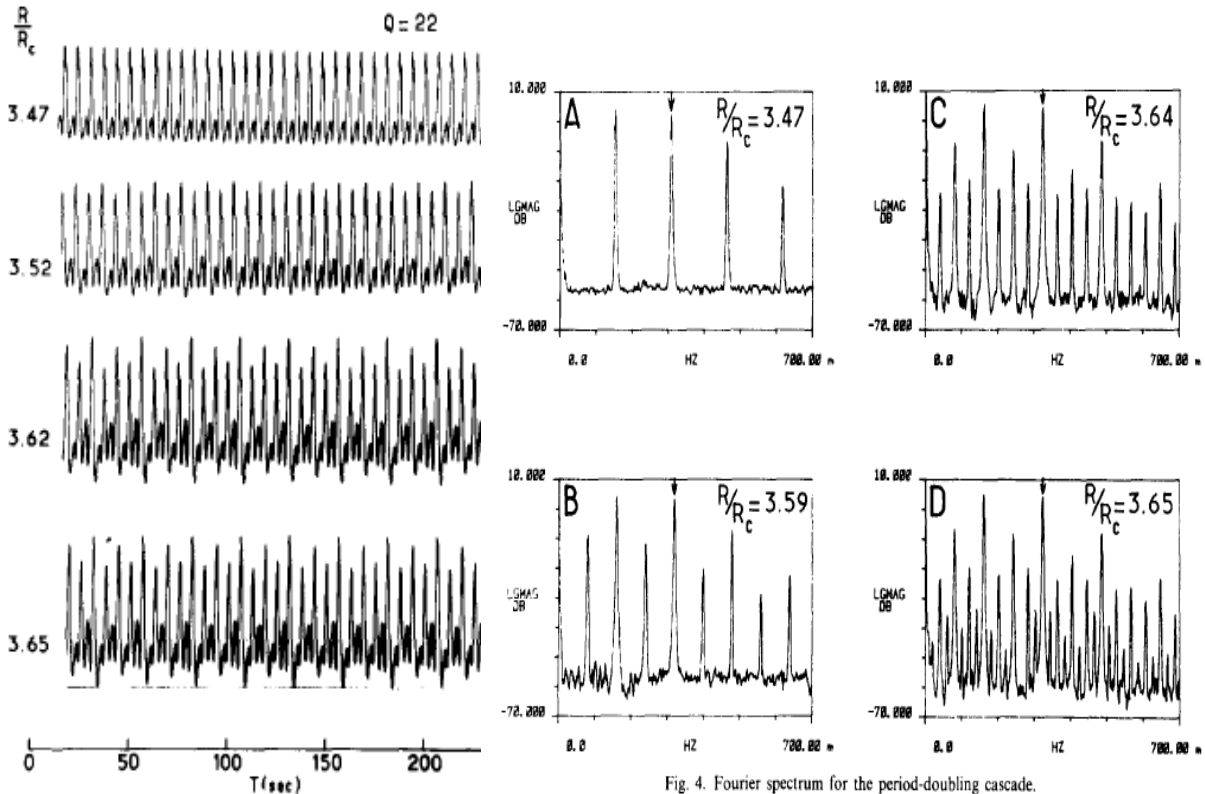

Fig. 3. The period doubling cascade ($\Gamma = 4$, $Q = 22$).

Fig. 4. Fourier spectrum for the period-doubling cascade.

Figure 12: Timeseries and power spectra from a Rayleigh-Bénard convection experiment with applied magnetic field in mercury. Timeseries show periods 2, 4, 8, 16. Power spectra show frequencies f and $f/2$ (A), $f/4$ (B), $f/8$ (C) and $f/16$ (D). Multiples of these frequencies are always present. From Libchaber, Fauve & Laroche, Physica D **7**, 73 (1983).

15

3.2 Lorenz system

Although the Lorenz system is not really fluid-dynamical, we will nevertheless discuss it here. Figure 13 shows a trajectory of the Lorenz system for the standard chaotic parameter value of $r = 28$. The trajectory jumps between the two lobes, as also seen on the timeseries of $X(t)$. One may make a *first return map* in the 3D (X, Y, Z) space by drawing a plane and retaining the crossings through the plane, e.g. $Z = r - 1$. Or one may choose successive maxima, e.g. $\dot{Z} = 0$, $\ddot{Z} < 0$. Either of these procedures defines a 2D discrete map. It may happen that the map is in fact 1D, because the dissipation is strong. This is seen in figure 14, in which successive maxima of Z are plotted, i.e. Z_{k+1} vs. Z_k. The fact that these lie on a curve instead of being scattered shows that the dynamics on the Lorenz attractor are effectively governed by a 1D mapping. This mapping has an unstable fixed point and resembles the tent map shown in figure 11.
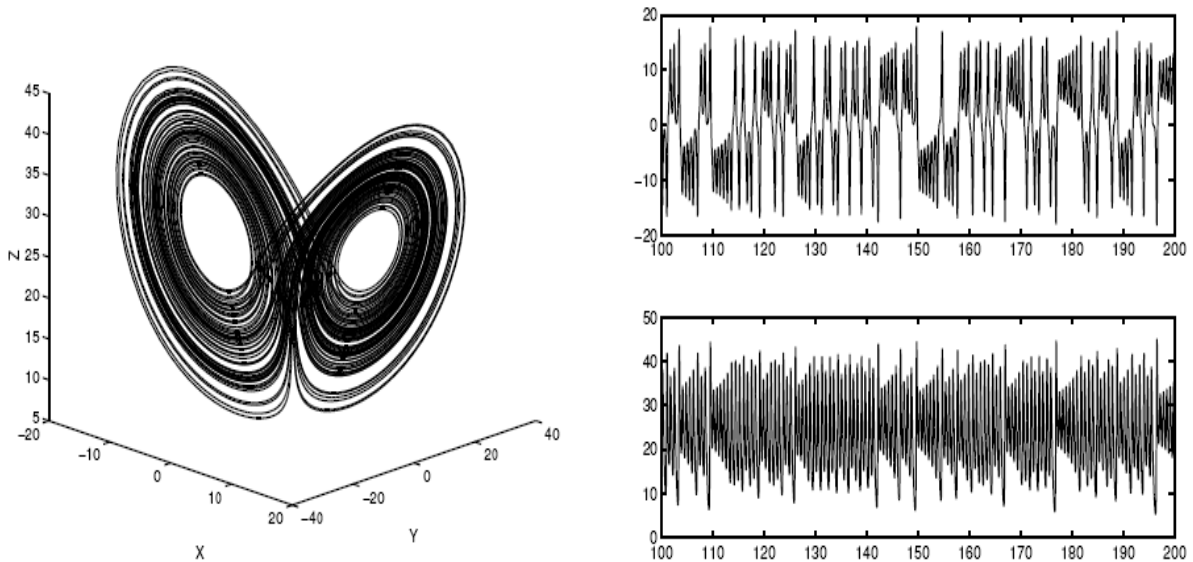

Figure 13: Left: 3D trajectory of the Lorenz system for standard chaotic value of $r = 28$. Right: corresponding timeseries. Above: timeseries of $X(t)$. Below: timeseries of $Z(t)$. From P. Manneville, Course notes.
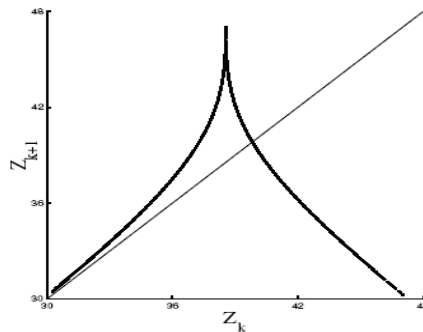

Figure 14: First return map for the Lorenz attractor. Successive pairs of maxima of Z are plottted. From P. Manneville, Course notes.

4 From continuous flows to discrete maps

Where do discrete dynamical systems come from? Often, they arise from limit cycles. Once a limit cycle has been created by one of the paths described in **Dynamical Systems**, that is, either a Hopf bifurcation or a global bifurcation, it too can undergo bifurcations and change stability, analogously to fixed points. The transformations undergone by a limit cycle are described in terms of maps.

4.1 Floquet Theory

The linear stability of a limit cycle is described by the mathematical framework of Floquet theory. A linear differential equation with constant coefficients such as

$$a\ddot{x} + b\dot{x} + cx = 0 \tag{37}$$

has as its general solution

$$x(t) = \alpha_1 e^{\lambda_1 t} + \alpha_2 e^{\lambda_2 t} \tag{38}$$

where $\lambda_{1,2}$ are the two solutions of the quadratic equation

$$a\lambda^2 + b\lambda + c = 0 \tag{39}$$

The solutions of first and N^{th} order linear differential equations are:

$$\dot{x} = cx \implies x(t) = e^{ct}x(0) \tag{40}$$

$$\sum_{n=0}^{N} c_n x^{(n)} = 0 \implies x(t) = \sum_{n=1}^{N} \alpha_n e^{\lambda_n t} \tag{41}$$

where $x^{(n)}(t)$ is the nth derivative of $x(t)$, $\{\lambda_n\}$ are the n roots of the equation

$$\sum_{n=0}^{N} c_n \lambda^n = 0 \tag{42}$$

and the coefficients α_n are determined by the initial and/or boundary conditions.

This form can be generalized to equations in which the coefficients are not constant, but periodic functions:

$$a(t)\ddot{x} + b(t)\dot{x} + c(t)x = 0 \tag{43}$$

a, b, c are all periodic functions with period T. The general solution of (43), analogous to (38), is

$$x(t) = \alpha_1(t)e^{\lambda_1 t} + \alpha_2(t)e^{\lambda_2 t} \tag{44}$$

Functions $\alpha_1(t)$, $\alpha_2(t)$ have the same period as $a(t)$, $b(t)$ and $c(t)$ and are called *Floquet functions*. The exponents λ_1 and λ_2 are called *Floquet exponents*. In contrast to the exponents in (38), these are not roots of a polynomial and must be calculated numerically or asymptotically. The values $\mu_1 \equiv e^{\lambda_1 T}$, $\mu_2 \equiv e^{\lambda_2 T}$ are called Floquet multipliers.

Similarly, we have, for the first and N^{th} order equations

$$\dot{x} = c(t)x \implies x(t) = e^{\lambda t}\alpha(t) \tag{45}$$

$$\sum_{n=0}^{N} c_n(t)x^{(n)} = 0 \implies x(t) = \sum_{n=1}^{N} e^{\lambda_n t}\alpha_n(t) \tag{46}$$

where the $\alpha_n(t)$'s have period T.

We now consider a dynamical system

$$\dot{x} = f(x) \tag{47}$$

which has as its solution a limit cycle of period T:

$$\bar{x}(t+T) = \bar{x}(t) \tag{48}$$

that is,

$$\dot{\bar{x}}(t) = f(\bar{x}(t)) \tag{49}$$

We now describe the evolution of a solution close to the limit cycle $\bar{x}$:

$$x(t) = \bar{x}(t) + \epsilon(t) \tag{50}$$

where $\epsilon(t)$ is assumed to remain small. Substituting (50) into (47), we obtain

$$\dot{\bar{x}} + \dot{\epsilon} = f(\bar{x}(t)) + f'(\bar{x}(t))\epsilon(t) + f''(\bar{x}(t))\epsilon(t)^2 + \dots \tag{51}$$

Taking (49) into account and neglecting higher order terms leads to

$$\dot{\epsilon} = f'(\bar{x}(t))\epsilon(t) \tag{52}$$

which is of the Floquet form (45). Therefore:

$$\epsilon(t) = e^{\lambda t}\alpha(t) \tag{53}$$

with $\alpha(t)$ periodic with period T. The limit cycle $\bar{x}(t)$ is stable if the real part of λ is negative. If λ is complex, this indicates that the period of the perturbation ϵ is different from that of the limit cycle $\bar{x}(t)$.

For a multidimensional system of dimension N, some of the equations above can be generalized to:

$$\dot{\epsilon} = Df(\bar{x}(t))\epsilon \tag{54}$$

$$\epsilon(t) = \sum_{j=1}^{N} e^{\lambda_j t}\alpha_j(t) \tag{55}$$

There are N Floquet exponents and Floquet functions and the limit cycle $\bar{x}$ is stable if all the real parts of the exponents are negative. The Floquet multipliers and Floquet functions are eigenvalues and eigenvectors of the *monodromy matrix* defined as follows. Let $M(t)$ be an $N \times N$ matrix whose evolution equation and initial condition are:

$$\dot{M} = Df(\bar{x}(t))M \qquad M(0) = I \tag{56}$$

$M(T)$ is the monodromy matrix. Thus, determining the Floquet exponents requires integrating the evolution equations linearized about $\bar{x}(t)$. The limit cycle $\bar{x}(t)$ is stable if all Floquet exponents have negative real parts.

In order for the imaginary part to be unique, we choose $Im(\lambda) \in (-\pi i/T, \pi i/T]$. (The remainder can be absorbed into the Floquet function.) See figure 15.
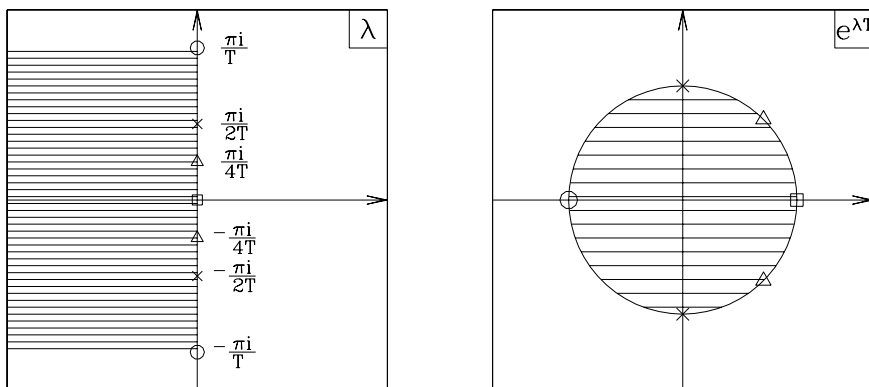
Figure 15: Region of stability for Floquet exponents λ (left) and for Floquet multipliers $e^{\lambda T}$ (right). The imaginary λ axis on the left is mapped into the unit circle on the right.
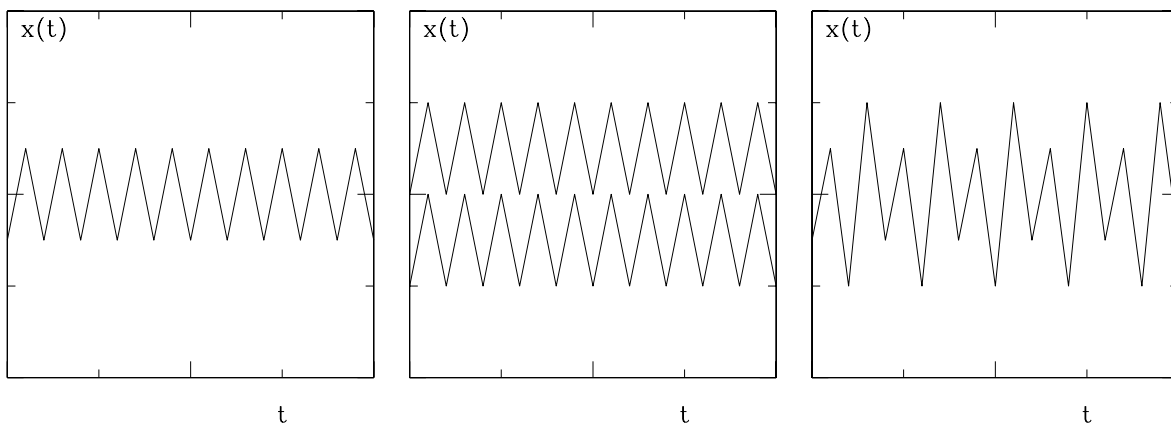

Figure 16: Schematic timeseries. The limit cycle (left) undergoes a pitchfork bifurcation (middle; the system will follow either the upper or the lower timeseries) or a period-doubling bifurcation (right).
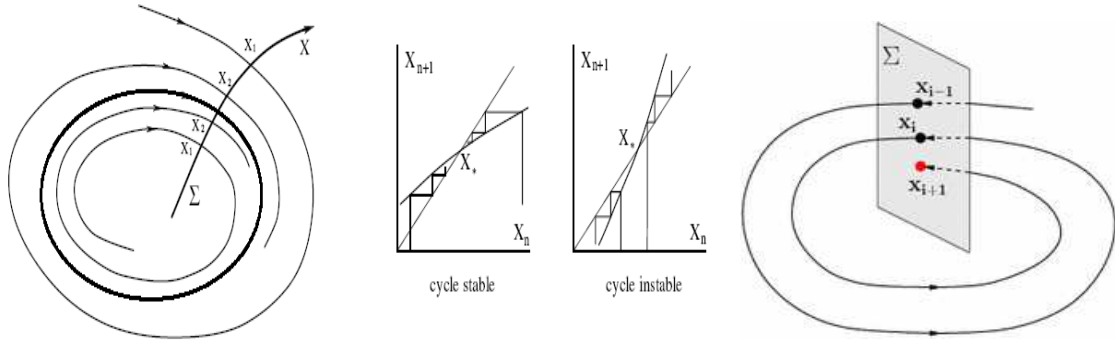
Figure 17: First return, or Poincaré mapping. Left: From P. Manneville, Class notes, DEA Physique des Liquides. Right: From Moehlis, Josic & Shea-Brown, Scholarpedia.

4.2 Poincaré Mapping

Figure 16 presents schematic timeseries following a pitchfork and a period-doubling bifurcation in figure 16.

To better understand the flow in the vicinity of a limit cycle (or a more complicated attractor), we can define a mapping, called the Poincaré map or first return map, as follows. Let $y \in \mathcal{R}^d$, and let y^d be the last component of y (any other component could be chosen instead). Let β be a value which x^d attains during the limit cycle. Let $x \in \mathcal{R}^{(d-1)}$, containing all but the dth component of x. We define:

$$x_{n+1} = g(x_n) \iff \begin{cases} y^d(t) = \beta, & \dot{y}^d(t) > 0, & y(t) = (x_n, \beta) \\ y^d(t') = \beta, & \dot{y}^d(t') > 0, & y(t') = (x_{n+1}, \beta) \\ y^d(t'') \neq \beta \text{ or } \dot{y}^d(t'') \leq 0 \text{ for all } t'' \in (t, t') \end{cases} \tag{57}$$

In order to avoid finding an appropriate value β, one can instead choose to select successive maxima of one of the components, i.e. $\dot{y}^d = 0$.

This defines a discrete dynamical system, or mapping, for $x \in \mathcal{R}^{d-1}$. The intersection of the trajectory $y(t)$ with the plane $y^d = \beta$ is mapped onto the next intersection (in the same direction). This construction is illustrated in figure 17, where a flow (continuous dynamical system) in d dimensions is reduced to a map (discrete dynamical system) in $d - 1$ dimensions.

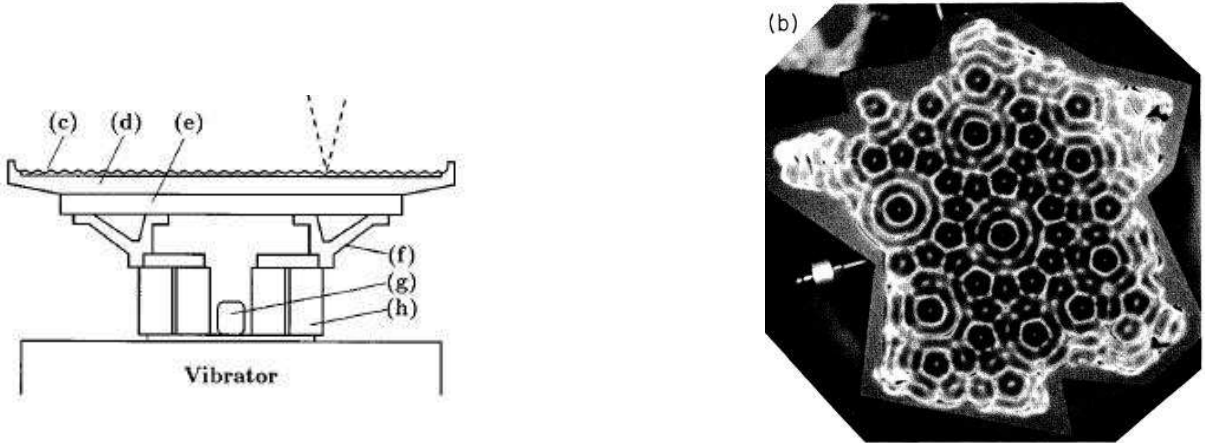# 5 Examples from fluid dynamics

5.1 Faraday instability

Figure 18: Left: experimental setup for Faraday experiment. Right: quasicrystalline pattern of surface waves obtained by vertically oscillating a fluid layer with a two-frequency forcing function. From Edwards & Fauve, J. Fluid Mech. **279**, 49 (1994).

In 1831, Faraday discovered that a pattern of standing waves was produced by vertical vibration of a thin fluid layer as in the left portion of figure 18. Lattice patterns of hexagons, squares, and rolls have been observed and, more recently, in the 1990s, more exotic flows such as quasicrystalline patterns and oscillons. A picture of a quasicrystalline pattern can be seen in figure 18.

The imposed vibration can be considered as an oscillatory boundary condition, but it is simpler to go into an oscillating frame of reference. The vibration then appears as an oscillatory gravitational force $G(t)$, which may be sinusoidal or more complicated:

$$G(t) = g\left(1 - a\cos(\omega t)\right) \tag{58}$$
$$G(t) = g\left(1 - [a\cos(m\omega t) + b\cos(n\omega t + \phi_0)]\right) \tag{59}$$

We wish to determine when and to what the flat surface becomes linearly unstable. The domain can be considered to be homogeneous in the horizontal directions if these are sufficiently large. The linear instability problem is therefore a constant-coefficient problem like (41) in the horizontal directions. Because the solutions must be bounded in the horizontal directions, the horizontal exponents are pure imaginary, i.e. the solutions are of the form $\exp(i\mathbf{k}\cdot\mathbf{x})$, or superpositions of these. Moreover, for a linear problem, solutions with different wavevectors $\mathbf{k}$ are decoupled and can be considered separately, and each depends only on $k = |\mathbf{k}|$. The vertical direction is neither homogeneous nor periodic, but can be eliminated via various manipulations. Therefore, the surface height variation ζ corresponding to perturbations of wavenumber k can be expanded as follows:

$$\zeta(x, y, t) = \sum_{\mathbf{k}} e^{i\mathbf{k}\cdot\mathbf{x}} \hat{\zeta}_k(t) \tag{60}$$

On the other hand, because of the oscillating gravitational force (or boundary), the linear instability

problem is a Floquet problem like (46) in time and so solutions $\hat{\zeta}_k(t)$ can be expanded

$$\hat{\zeta}_k(t) = \sum_j e^{\lambda_k^j t} f_k^j(t) \tag{61}$$

where the functions $f_k^j(t)$ are periodic with period T and λ_k^j are the Floquet exponents.

If the fluids are ideal (no viscosity) and the forcing is sinusoidal, then the height can be shown to be governed by the classic *Mathieu equation*:

$$\partial_{tt}\hat{\zeta}_k + \omega_0^2 \left[1 - a\cos(\omega t)\right]\hat{\zeta}_k = 0 \tag{62}$$

where ω_0^2 is a parameter combining the densities of the upper and lower fluids, the surface tension, the wavenumber k and the gravitational acceleration g.

The Floquet multipliers are $\mu_k^j \equiv e^{\lambda_k^j T}$. If one of the $|\mu_k^j|$ exceeds one for some k, then $\hat{\zeta}_k$ grows in time, the flat surface is unstable, and Faraday waves occur. As a parameter – the amplitude a or frequency ω of the imposed vibration or the wavenumber k – is varied, a Floquet multiplier exits the unit circle either at 1 or at -1; for this problem, it can be shown that the instability cannot be via a complex multiplier. When the Floquet multiplier is -1, the period of the surface waves is twice that of the imposed oscillation in G; the waves are said to be *subharmonic*. When the Floquet multiplier is $+1$, the period of the surface waves is the same as that of G and the waves are said to be *harmonic*. For most experimental parameters, the Faraday instability observed is in fact subharmonic. The analysis is illustrated in figures 19, 20 and 21.
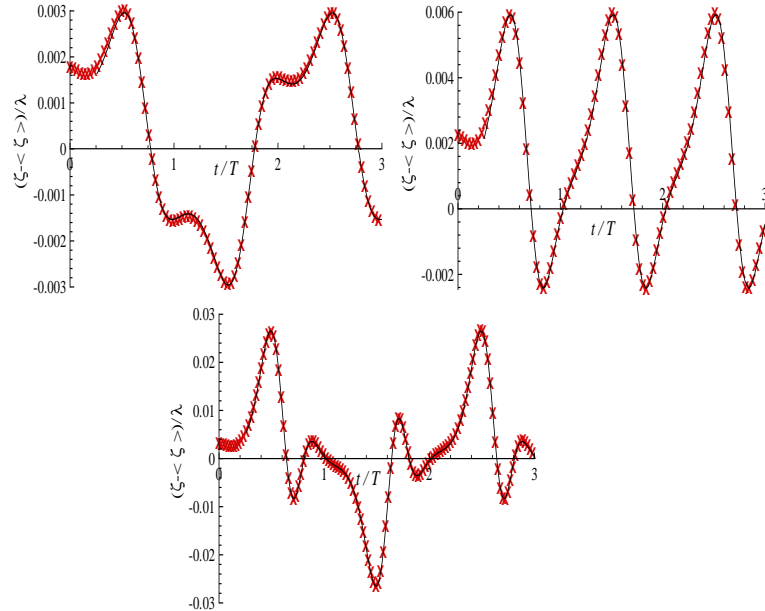

Figure 19: Floquet functions for values of k within tongues 1/2 (left), 1 (middle) and 3/2 (right). The function from tongue 1 is harmonic: its period is the same as that of the forcing. The functions from tongues 1/2 and 3/2 are subharmonic: their period is twice that of the forcing. From Périnet, Juric & Tuckerman, J. Fluid Mech. **635**, 1–26 (2009).
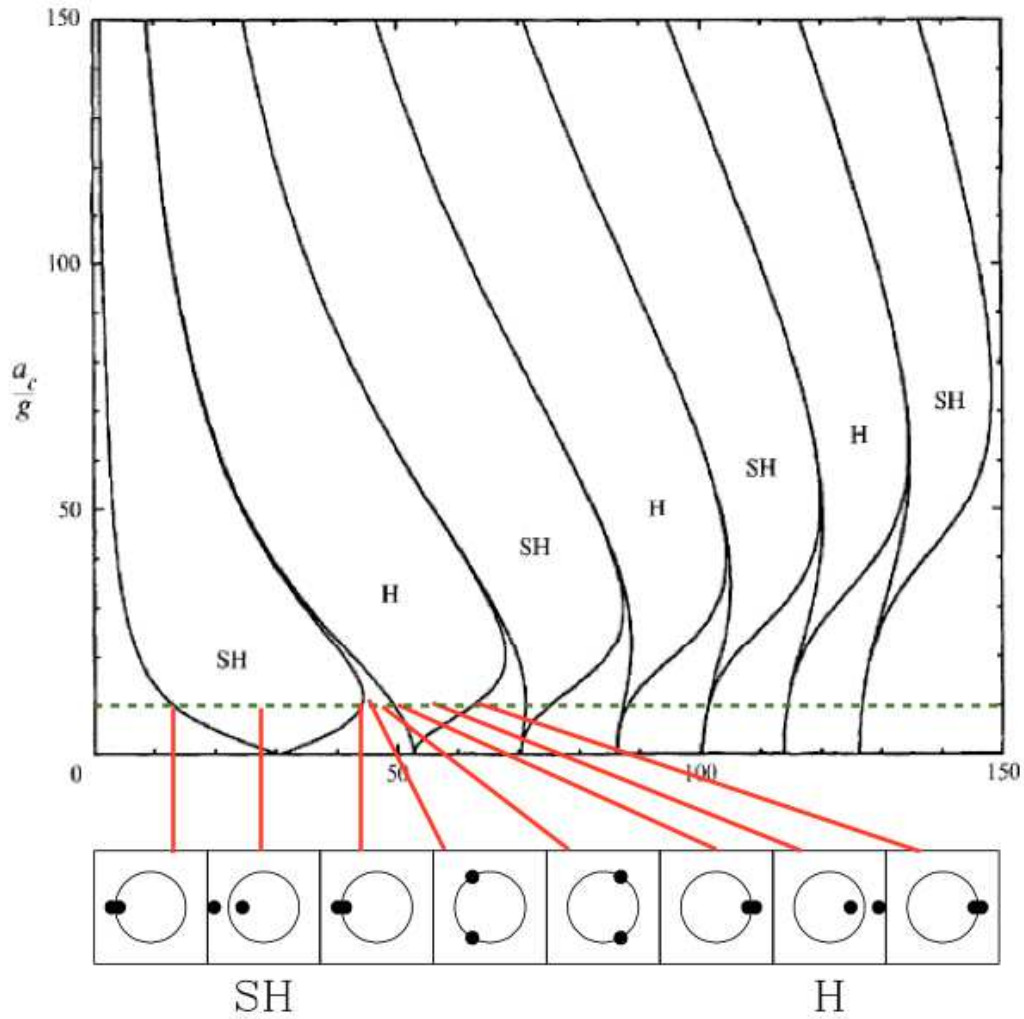
Figure 20: Instability tongues for the Faraday problem in an inviscid fluid. Inside the tongues, one of the Floquet multipliers μ exceeds one in absolute value. In a harmonic tongue (H), $\mu > 1$ for some μ, while in a subharmonic tongue (SH) $\mu < -1$. From Kumar & Tuckerman, J. Fluid Mech. **279**, 49 (1994).
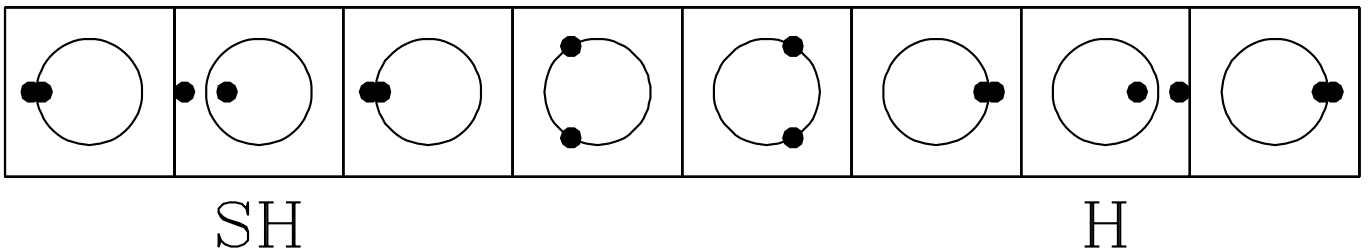

Figure 21: Schematic diagram of location of a pair $\mu_\pm$ of Floquet multipliers as a parameter is varied, for example k in the figure above. Inside a subharmonic (SH) tongue, $\mu_\pm \approx -1 \pm c$. The two multipliers leave -1 in opposite directions along the real axis. They then approach one another along the real axis, meeting at -1 (the right boundary of the subharmonic tongue). They then leave -1 in opposite directions along the circle. Outside of any tongue, $\mu_\pm \approx e^{\pm i\theta}$. They meet again at $+1$ (left boundary of the harmonic tongue) and leave in opposite directions along the real axis. Inside a harmonic (H) tongue, $\mu_\pm \approx 1 \pm c$.
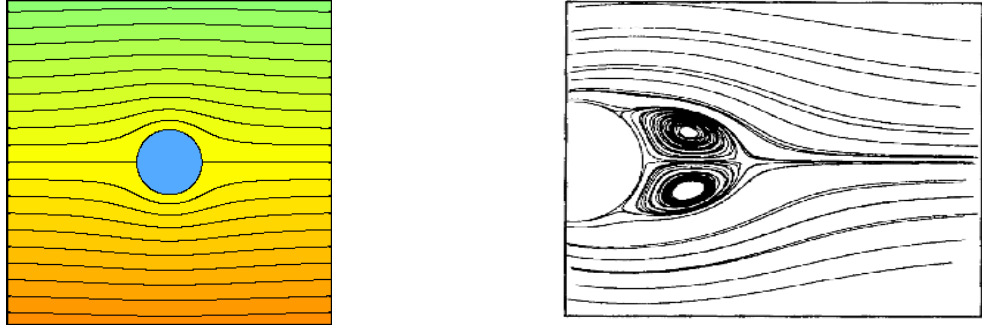
5.2 Cylinder wake: Floquet analysis

Figure 22: Flow around a circular cylinder. Ideal flow (left) and with downstream recirculation zone (right).

Figure 23: Von Kármán vortex street in the laboratory (left, Taneda, 1982) and in nature (right, off Chilean coast, past Juan Fernandez islands).

The wake of a circular cylinder is a classic problem in fluid dynamics. When a stationary cylinder is placed in a uniform flow perpendicular to its axis, the streamlines curve around the cylinder, as in the left portion of figure 22. At higher Reynolds number (defined from the uniform background flow, the cylinder diameter, and the viscosity of the fluid) a recirculation zone appears downstream, as in the right portion of figure 22. When the Reynolds number surpasses a critical value, vortices appear, as shown in figure 23. The vortices are of alternating sign, appear on alternating sides of the cylinder, and travel downstream. This structure is called the *von Kármán vortex street* and the non-dimensionalized frequency of vortex shedding is called the Strouhal number St.

In terms of dynamical systems, the von Kármán vortex street is a limit cycle created from the steady flow by a Hopf bifurcation. In the idealized situation of a cylinder of infinite length, the flow is two-dimensional, with no variation along the cylinder axis (called the spanwise direction). For yet a higher value of Re, von Kàrmàn vortex street itself becomes unstable and the flow becomes three-dimensional, as shown in figure 24. The loss of stability of the time-periodic von Kármán vortex street is a Floquet problem. Unlike the case of the Faraday instability, the time-periodicity is not forced by the experimentalist, but emerges spontaneously from the temporally homogeneous conditions (cylinder in uniform flow).

The stability analysis proceeds as follows. The limit cycle, i.e. the 2D von Kármán vortex street,

$\mathbf{U}_{2D}(x, y, t)$ the limit cycle is a periodic time-dependent solution to the Navier-Stokes equations:

$$\partial_t \mathbf{U}_{2D} = -(\mathbf{U}_{2D} \cdot \nabla)\mathbf{U}_{2D} - \nabla P_{2D} + \frac{1}{Re}\Delta\mathbf{U}_{2D} \tag{63}$$

The domain is taken to be very large in the (x, y) directions. The velocity is zero on the surface of the cylinder and equal to the imposed uniform flow at infinity.

The perturbation $\mathbf{u}_{3D}$ is a solution to the Navier-Stokes equations linearized about $\mathbf{U}_{2D}(t)$:

$$\partial_t \mathbf{u}_{3D} = -(\mathbf{U}_{2D}(t) \cdot \nabla)\mathbf{u}_{3D} - (\mathbf{u}_{3D} \cdot \nabla)\mathbf{U}_{2D}(t) - \nabla p_{3D} + \frac{1}{Re}\Delta\mathbf{u}_{3D} \tag{64}$$

The perturbed velocity obeys homogeneous boundary conditions on the surface of the cylinder and at infinity. Equation (64) is homogeneous in the spanwise direction z (along the cylinder). Since we require that solutions be bounded, the solutions are trigonometric, of form $e^{i\beta z}$, and the solution for each β evolves independently of the others. Equation (64) is a Floquet problem in time t via the periodic flow $\mathbf{U}_{2D}(t)$ about which we linearize. We can therefore decompose $\mathbf{U}_{3D}(t)$ into

$$\mathbf{u}_{3D} \sim e^{i\beta z} e^{\lambda_\beta t} \mathbf{f}_\beta(x, y, t) \tag{65}$$

where the Floquet functions $\mathbf{f}_\beta(x, y, t)$ are periodic in time and the Floquet multipliers are $\mu_\beta = e^{\lambda_\beta T}$. For each β, there is a set of Floquet functions and multipliers. The largest are computed numerically and used to determine the stability of the von Kármán vortex street $\mathbf{U}_{2D}(t)$, in particular the wavenumber β and Reynolds number at which the modulus of one of the multipliers $|\mu_\beta|$ first exceeds one in modulus.

This Floquet analysis was carried out numerically by Barkley and Henderson in 1995-6. There are actually two bifurcations, to modes with different wavenumbers β at different Reynolds numbers Re, as shown in figure 24. It turns out that the limit cycle undergoes a *steady* bifurcation, i.e. μ traverses the unit circle at 1, not at -1 nor at $e^{\pm i\theta}$, as shown in figure 25. Thus, the temporal behavior of the new 3D solutions is similar to that of the 2D flow. The bifurcation is a circle pitchfork, in that any spatial phase in z is permitted.

The 3D transitions of the cylinder wake illustrate several other bifurcation phenomena. First, the bifurcation to mode A is slightly subcritical, while that to mode B is supercritical. This can actually be determined by using a single timeseries near the bifurcation. Figure 26 shows that both transitions begin with exponential growth, at the rate of the computed Floquet multiplier and then deviate from the exponential curve. However, when the transition to mode A first deviates, it is *above* the exponential curve, i.e. the nonlinear effects initially increase the instability. In contrast, when the transition to mode B first deviates, it is *below* the exponential curve, i.e. the nonlinear effects initially decrease. We write the dynamical system governing the transitions as

$$A_{n+1} = \left(\mu_A + \alpha_A|A_n|^2\right)A_n \tag{66}$$
$$B_{n+1} = \left(\mu_B + \alpha_B|B_n|^2\right)B_n \tag{67}$$

where A_n, B_n represent modes A and B at the same instant in the von Kármán vortex shedding period. The complex coefficients describe the amplitude and spanwise phase of a state produced by a circle pitchfork. Figure 26 shows that $\alpha_A > 0$, while $\alpha_B < 0$. In order to saturate mode A, a fifth-order term must be added:

$$A_{n+1} = \left(\mu_A + \alpha_A|A_n|^2 A_n + \beta_A|A_n|^4\right)A_n \tag{68}$$
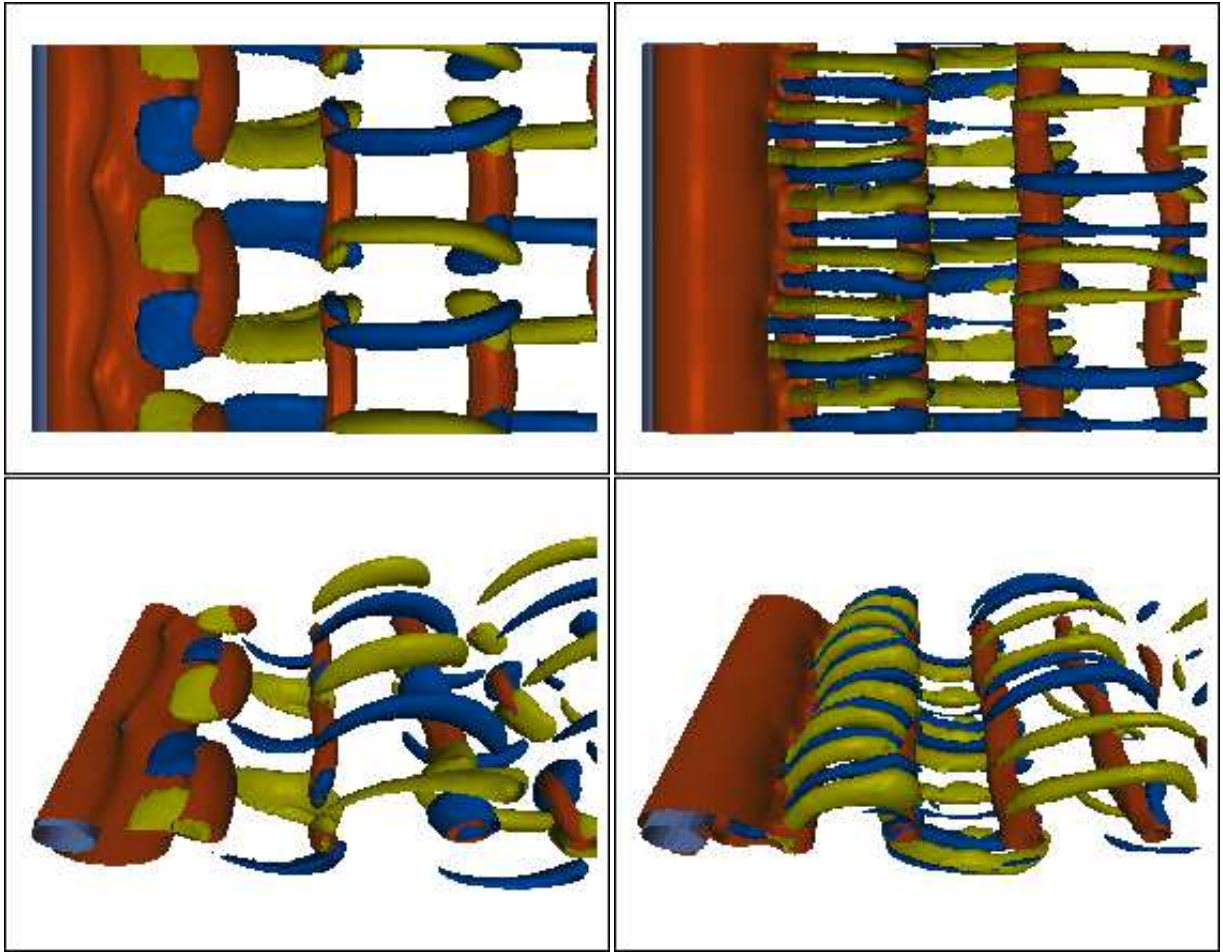
where $\beta_A < 0$.

Figure 24: Three-dimensional flow past a cylinder. Left: at $Re = 210$, mode A with a wavelength near four times the cylinder diameter. Right: at $Re = 250$, mode B with a wavelength near the cylinder diameter. From M.C. Thompson, Monash University, Australia. (http://mecmail.eng.monash.edu.au/~mct/mct/docs/cylinder.html)
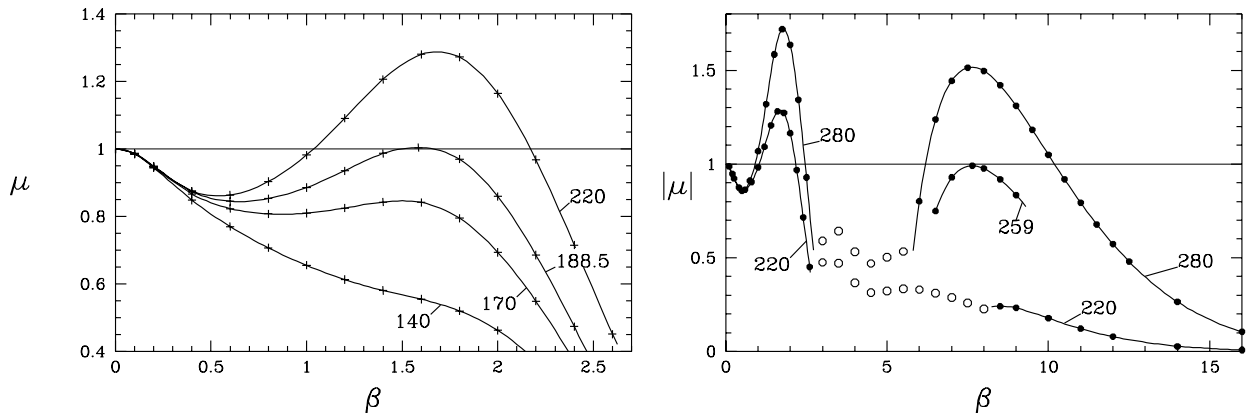

Figure 25: Floquet multipliers as a function of Reynolds number Re and spanwise wavenumber β. Left: Onset of instability to mode A ($\mu = 1$) at $Re = 188.5$ and $\beta = 1.585$. (wavelength $2\pi/\beta = 3.96$). Right: Onset of instability to mode B ($\mu = 1$) for $Re = 259$ and $\beta = 7.64$ (wavelength $2\pi/\beta = 0.822$). From Barkley & Henderson, J. Fluid Mech. **322**, 215 (1996).
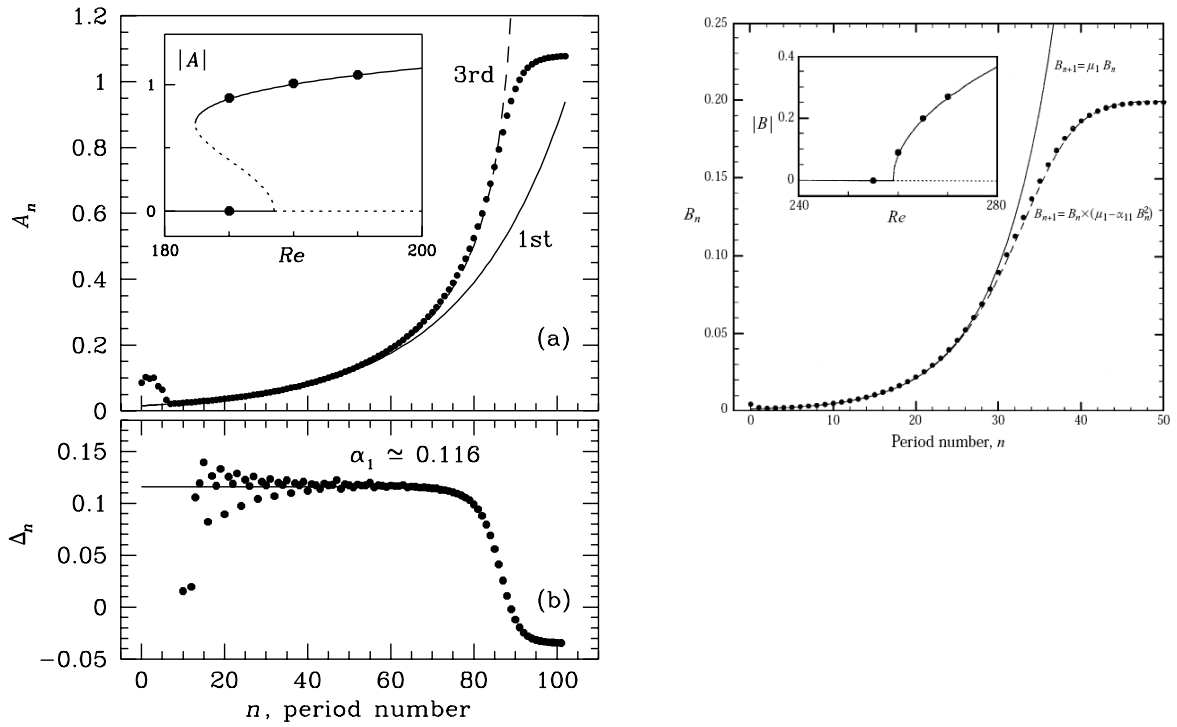
Figure 26: Transition in time to mode A (left) and mode B (right). Both transitions begin with exponential growth at the rate of the computed Floquet multiplier. Mode A then grows faster than exponentially, indicating a subcritical bifurcation, while mode B grows slower than exponentially, indicating a supercritical bifurcation.

Figures 27 and 28 show that, when increasing Re, mode A is observed, then a mixture of modes A and B, and finally mode B. These figures show experimental measurements and modes A and B are identified by their characteristic spatial wavelength and temporal frequency. These facts imply that modes A and B interact. Their symmetries can be taken into account to determine the invariants and equivariants. A minimal set of equations reproducing the behavior of the transitions is:

$$A_{n+1} = \left(\mu_A + \alpha_A |A_n|^2 + \gamma_A |B_n|^2 + \beta_A |A_n|^4 \right) A_n \qquad (69)$$

$$B_{n+1} = \left(\mu_B + \alpha_B |B_n|^2 + \gamma_B |A_n|^2 \right) B_n \qquad (70)$$

Nonlinear simulations of the 3D Navier-Stokes equations can be used to determine the values of α, β and γ. Solutions to this minimal model (69)-(70) with these coefficients are shown in figure 29.
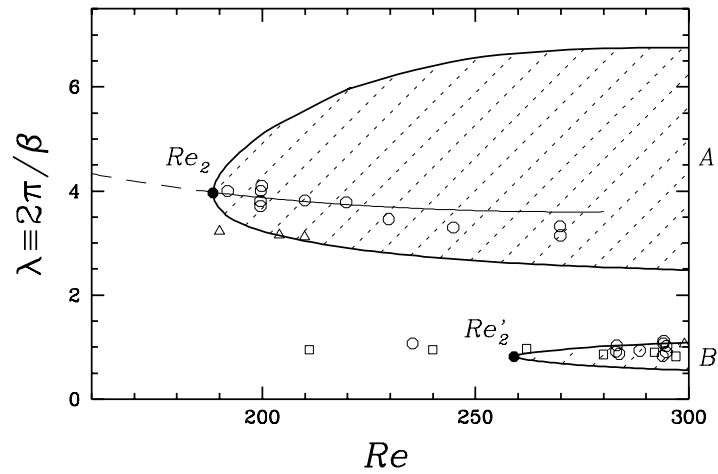
Figure 27: Region of instability in (Re, β) plane. Curves and shaded region from numerical Floquet analysis. Symbols show experimental observations. From Barkley & Henderson, J. Fluid Mech. **322**, 215 (1996).
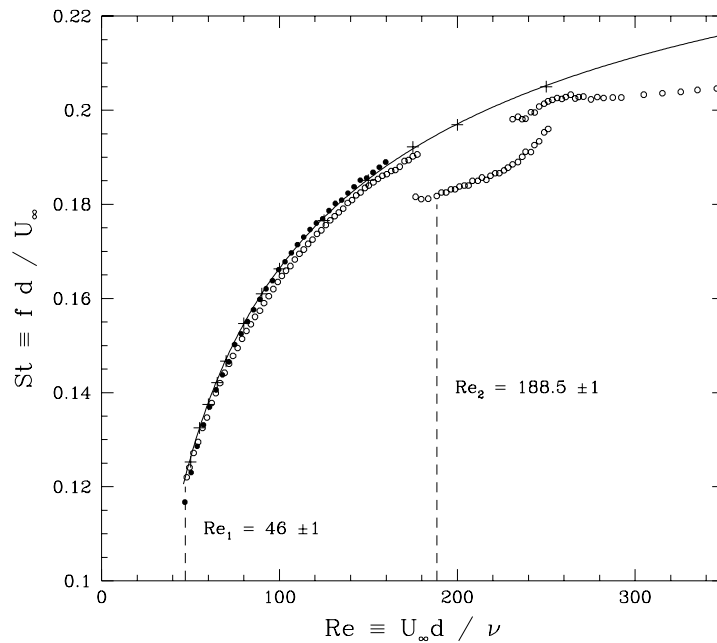

Figure 28: Strouhal number (frequency) as a function of Re. Curve from 2D computations. Symbols show experimental observations. From Barkley & Henderson, J. Fluid Mech. **322**, 215 (1996).
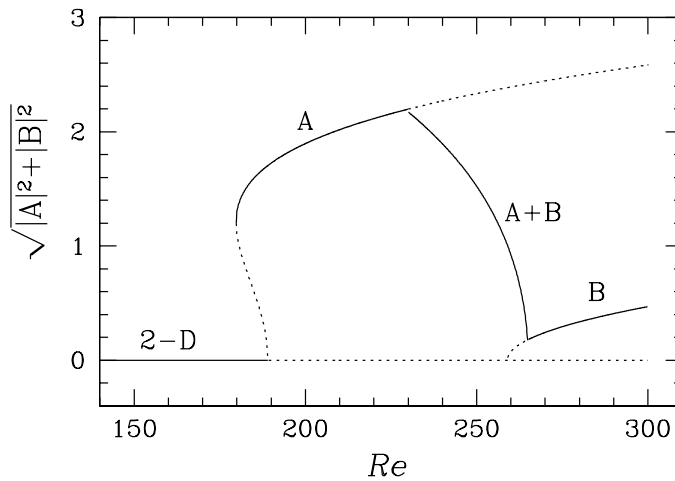

Figure 29: Solution to minimal model. From Barkley, Tuckerman & Golubitsky, Phys. Rev. E **61**, 5247 (2000).

Exercises on Discrete Maps

1. Consider the discrete-time dynamical system

$$x_{n+1} = f(x_n) = \alpha x_n + x_n^3$$

The parameter α may take on positive or negative values.

a. Determine the fixed points and their stability.

b. Determine the location and nature of bifurcations undergone by the fixed points and describe the new states resulting from the bifurcations.

c. Draw the corresponding bifurcation diagram plotting x as a function of α, indicating stable and unstable branches and labeling each bifurcation.

2. The logistic map $f(x) = rx(1 - x)$ undergoes a bifurcation to a three-cycle at $r_c = 1 + \sqrt{8}$. Show this as follows.

a. The three-cycle with elements a, b, c is produced by a saddle-node bifurcation of f^3. Hence $d(f^3(x))/dx = 1$ at $r = r_c$ and $x = a$. Using the chain rule, write this as an equation relating r_c, a, b, c. Rewrite this equation in terms of $\alpha \equiv a + b + c$, $\beta \equiv ab + bc + ac$ and $\gamma \equiv abc$.

b. Since $f(x)$ has a three-cycle, $f^3(x)$ has fixed points, and so the function $g(x) \equiv f^3(x) - x$ has roots at $x = a, b, c$. At the bifurcation point $r = r_c$, these are double roots. (For $r > r_c$, there are three other roots a', b', c' belonging to an unstable three-cycle.) $g(x)$ also has roots at the fixed points of $f(x)$, which are $x = 0$ and $1 - 1/r$. Using this, write $g(x)$ as a product of linear factors, with an unknown constant of proportionality. Multiply these linear factors together to get a polynomial in terms of the constants α, β, γ given above. For the polynomial form, only the terms in x^8, x^7, x^6, x^5 will be explicitly needed in what follows.

c. Write out the form of $g(x)$ directly from its definition $g(x) \equiv f^3(x) - x$ with $f(x) = rx(1 - x)$. Again, only the terms in x^8, x^7, x^6, x^5 will be needed.

d. Match the coefficients of g from the expressions in part **b, c** above to derive expressions for α, β, γ in terms of r.

e. Substitute these expressions into the equation obtained in part **a** and obtain the expression for r_c.